ACS Photonics

Article

pubs.acs.org/journal/apchd5

Optical Response of Hybrid Plasmon−Exciton Nanomaterials in the Presence of Overlapping Resonances

Maxim Sukharev,*[,†] Paul N. Day,[‡] and Ruth Pachter*[,‡]

[†]Science and Mathematics Faculty, College of Letters and Sciences, Arizona State University, Mesa, Arizona 85212, United States

[‡]Materials and Manufacturing Directorate, Air Force Research Laboratory, Wright-Patterson Air Force Base, Dayton, Ohio 45433, United States

ABSTRACT: We consider a hybrid plasmon−exciton system comprising a resonant molecular subsystem and three Au wires supporting a dipole mode that can be coupled to a dark mode in controllable fashion by variation of a symmetry parameter. The physics of such a system under strong coupling conditions is examined in detail. It is shown that if two wires supporting the dark mode are covered with molecular layers, the system exhibits four resonant modes for a strong coupling regime due to asymmetry and lifted degeneracy of the molecular state in this case, while upon having molecular aggregates covering the top wire with a dipolar mode, three resonant modes appear. Pump−probe simulations are performed to scrutinize the quantum dynamics and find possible ways to control plasmon−exciton materials. It is demonstrated that one can design hybrid nanomaterials with highly pronounced Fano-type resonances when excited by femtosecond lasers.

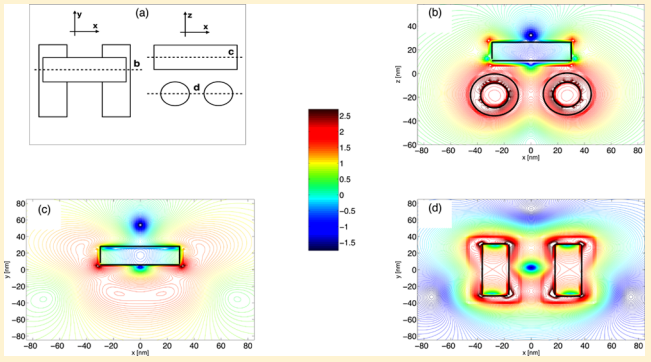

KEYWORDS: *exciton−plasmon coupling, surface plasmons, Fano resonance*

Understanding plasmon−exciton or so-called plexitonic coupling[1] in hybrid plasmonic nanostructures is important for tuning the optical response, e.g., for applications in nonlinear optics,[2] organic solar cells,[3] or organic light-emitting diodes.[4] In developing such nanostructures, it is important to consider strong coupling phenomena. Indeed, experimentally, Rabi oscillations were observed in J-aggregate/metal nanostructures.[5−8] For example, in the work by Schlather et al.,[8] gold nanodisk dimers were utilized, with J-aggregates formed from monomers of a cyanine dye. Cynanine dyes were also used in the work by DeLacy et al.[5] with silver nanoplatelets. Limiting cases of Rabi oscillations/Fano resonances were identified, where the plasmon resonance has an extremely narrow/large line width.[9]

Inducing a Rabi splitting, for example, could be useful in gaining increased tunability in the response. However, such tunability is limited, e.g., in varying the distance between dimers. Here we consider an asymmetric metal plasmonic nanostructure in conjunction with a quantum excitonic subsystem and particularly the effects of the excitonic subsytem on the coupling between the dipolar and quadrupole modes. We adopted the geometry similar to that described by Gallinet et al.[10] by varying the symmetry parameter. In previous works, we considered plexitonic nanomaterials in both linear[11] and nonlinear[12,13] regimes. It was shown that in addition to commonly observed Rabi splittings plexitonic systems exhibit collective resonances at high exciton densities. Such resonances correspond to collective electromagnetic modes induced by strong exciton−exciton interactions greatly enhanced by plasmons.[11] The existence of plasmon-enhanced collective exciton modes has also been confirmed in core−shell materials.[14] Moreover using the pump−probe technique one can modify optical properties of plexitonic structures via modifications of exciton populations[12] and efficiently control electromagnetic localization in both space and time.[13]

Using a self-consistent rigorous approach, we show that upon strong coupling in the asymmetric structure similar to the one in ref 10, and with inclusion of a strongly coupled excitonic subsystem, also varying the position of deposition, interesting phenomena appear that have not been elucidated yet. Such systems improve on the tunability of plexitonic hybrid materials. Furthermore, in performing pump−probe simulations we note the appearance of a highly pronounced Fano line shape.

The appearance of Fano resonances in nanosystems, in general,[15] and dolmen-like plasmonic structures, in particular,[16,17] has long attracted considerable attention due to various applications. In this article we demonstrate that such resonances can be induced by strong femtosecond laser pulses applied to a hybrid material, resulting in systems exhibiting strong optical absorption in the visible, which could find application in active optoelectronic devices.[18]

Received: March 25, 2015
Published: June 3, 2015

DOI: 10.1021/acsphotonics.5b00146
ACS Photonics 2015, 2, 935−941

THEORETICAL MODEL

The spatiotemporal dynamics of electric, $\vec{E}$, and magnetic, $\vec{H}$, fields is considered classically using the full machinery of the Maxwell equations

$$\mu_0 \frac{\partial \vec{H}}{\partial t} = -\nabla \times \vec{E} \tag{1a}$$

$$\varepsilon_0 \frac{\partial \vec{E}}{\partial t} = \nabla \times \vec{H} - \vec{J} \tag{1b}$$

where ε_0 and μ_0 are the permittivity and the permeability of the free space, respectively, and $\vec{J}$ corresponds to either the current density in spatial regions occupied by metal or the macroscopic polarization current, $\vec{J} = \partial\vec{P}/\partial t$, in space with molecules. Equations 1 are integrated using the finite-difference time-domain (FDTD) approach, which implicitly accounts for Gauss's law via Yee's cell, thus requiring only two equations to solve.

To account for the material dispersion in a metal, the Drude model is implemented. In this model the current density is evaluated according to the following equation:[19]

$$\frac{\partial \vec{J}}{\partial t} + \Gamma \vec{J} = \varepsilon_0 \omega_p{}^2 \vec{E} \tag{2}$$

where Γ is the damping parameter and ω_p is the bulk plasma frequency. An additional parameter that enters the Drude model is the high-frequency limit of the dielectric constant ε_r. For the range of frequencies considered in this work the following set of parameters was chosen to represent gold: ε_r = 9.5, ω_p = 8.95 eV, and Γ = 0.069 eV. We note that we tested a more precise description of the dielectric function of gold using the Drude–Lorentz model.[20] The results were qualitatively similar to those obtained with the Drude model; that is, all resonances discussed below were present, but their energy positions were slightly different. Moreover the physical nature of all resonances was the same as we checked via calculating corresponding charge distributions. The Drude model, however, leads to significantly shorter execution times of our codes; hence it was used to capture essential physics rather than quantitative features.

The optical response of a molecular aggregate is simulated using rate equations for a two-level system[21] driven by a local electric field $\vec{E}$:

$$\frac{dn_1}{dt} - \gamma_{21} n_2 = -\frac{1}{\hbar\Omega_0} \vec{E} \frac{\partial \vec{P}}{\partial t} \tag{3a}$$

$$\frac{dn_2}{dt} + \gamma_{21} n_2 = \frac{1}{\hbar\Omega_0} \vec{E} \frac{\partial \vec{P}}{\partial t} \tag{3b}$$

$$\frac{\partial^2 \vec{P}}{\partial t^2} + (\gamma_{21} + 2\gamma_d) \frac{\partial \vec{P}}{\partial t} + \Omega_0^2 \vec{P} = -\sigma(n_2 - n_1)\vec{E} \tag{3c}$$

where n_1 and n_2 describe the populations of the ground and the excited molecular states, respectively, $\vec{P}$ is the macroscopic polarization, γ_{21} is the radiationless decay rate of the excited state, γ_d is the pure dephasing rate, and $\hbar\Omega_0$ is the energy separation of the molecular levels. The coupling constant σ can be derived from a simple harmonic oscillator, as readily shown in ref 22.

$$\sigma = \frac{2\Omega_0 \mu_{12}}{3\hbar} \tag{4}$$

where μ_{12} is the transition dipole moment.

Equations 1 and 3 are coupled via polarization current $\vec{J} = \partial\vec{P}/\partial t$, which appears in the Ampere law. The resulting system of equations is solved numerically on a multiprocessor computer. We note that in such an approach the static molecule–molecule interactions are neglected, thus allowing us to treat each molecule independently. This method, however, does account for all interactions between molecules that are induced by external EM radiation. The values of the molecular parameters used in this work are μ_{12} = 10 D, $\gamma_{21} = 6.892 \times 10^{-4}$ eV (corresponding to 6 ps), and $\gamma_d = 6.565 \times 10^{-3}$ eV (corresponding to 630 fs), and the total number density of molecules is $n_0 = 4 \times 10^{25}$ m^{-3}. The thickness of a molecular layer in all simulations below is 10 nm. Finally we assume that the dielectric host for all structures considered in this work has a dielectric constant ε = 1.7689, corresponding to that of water.

The space is discretized in accordance with the FDTD algorithm[23] in three dimensions. The spatial resolution is $\delta x = \delta y = \delta z$ = 1.5 nm to achieve numerical convergence and avoid staircase effects. To ensure numerical convergence for pump–probe simulations as discussed in detail in the section Pump–Probe Simulations, we repeated several runs with a spatial resolution of 1.0 and 0.8 nm. The results were nearly identical to those obtained with a 1.5 nm step. The time step is $\delta t = \delta x/2c$ = 2.5 as, where c is the speed of light in a vacuum. Open boundaries are simulated using convolutional perfectly matched layers (CPMLs).[24] We found that for systems considered here the best results were achieved with 19 CPMLs.

The excitation of a system is carried out using the total field/scattered field approach,[23] which allows one to inject a plane wave into a simulation domain. For calculations of linear spectra we employ a short-pulse method[25] with a time pulse envelope, $f(t)$, written in the form of the Blackman–Harris window:

$$f(t) = \sum_{n=-0}^{3} a_n \cos\left(\frac{2\pi n t}{\tau}\right) \tag{5}$$

for a pulse with a duration τ, where a_0 = 0.353 222 222, a_1 = −0.488, a_2 = 0.145, and a_3 = −0.010 222 222. The same time envelope was used to simulate a femtosecond pump.

To test our numerical approach, we qualitatively compare results of our simulations with data from ref 10. The structure considered in this work is schematically depicted in the inset of Figure 1. To characterize this system, we place a pointwise detector above the upper wire and compute the EM energy flux in the positive z direction. The subsequent normalization of these calculations to the energy flux of the incident wave results in reflection, as plotted in the main panel of Figure 1.

The upper wire acts as a dipole antenna coupling to incident radiation. The bottom two wires support a dark mode that cannot be directly excited by the external field. The dipole antenna, however, depending on the asymmetry parameter S (see the inset in Figure 1), allows one to harvest the dark mode. The main panel shows the reflection calculated at a point near the system. It is seen from this figure that the more asymmetric the structure is, the stronger the coupling between the dipole mode of the upper wire and the dark mode of the two parallel wires. This observation is in a good agreement with the main results of ref 10. We note that the dipole mode for the upper

DOI: 10.1021/acsphotonics.5b00146
ACS Photonics 2015, 2, 935–941

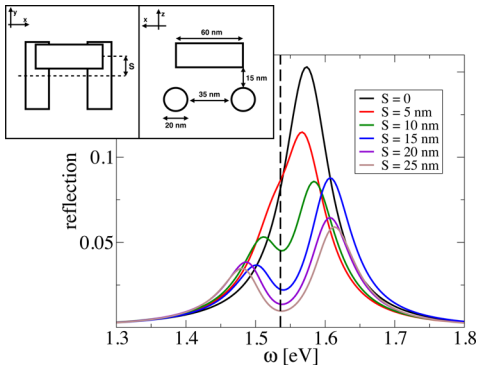

Figure 1. Inset shows the arrangement of gold nanowires in a three-dimensional structure. The system is excited by a plane wave polarized along the *x*-axis and propagating along the negative *z* direction. The fixed geometrical parameters such as the length of each wire are indicated in the inset. The main panel shows reflection spectra for the system as a function of the incident photon energy at different positions of the upper wire as indicated in the main panel legend. The vertical dashed line shows the position of the quadrupole mode at 1.53574 eV.

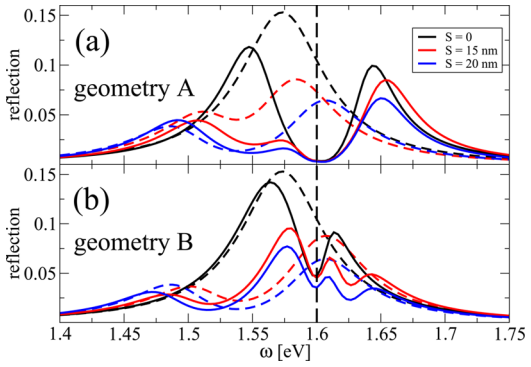

Figure 2. Reflection spectra for two scenarios of a deposition of molecular aggregates. (a) Results as solid lines for the molecular layer covering the upper wire (see the inset in Figure 1 for details). (b) Data as solid lines obtained with two lower wires covered by resonant molecules. In both scenarios the thickness of a molecular layer is 10 nm with all molecules resonant at Ω_0 = 1.6 eV, as indicated by the vertical dashed line. Dashed lines in both panels correspond to reflection spectra without molecular aggregates.

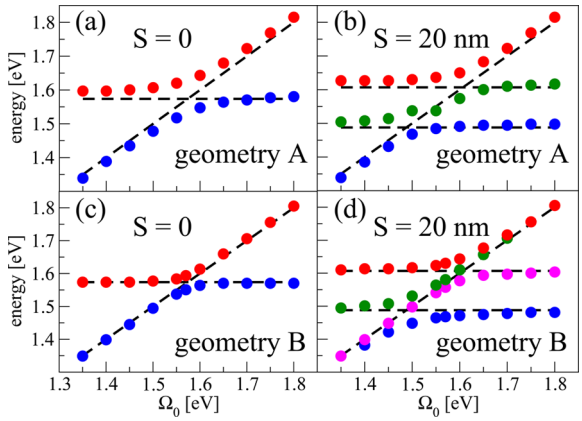

Figure 3. Avoided crossings for two sets of geometries. Panels (a) and (b) show energy positions of all resolved resonances in reflection spectra as functions of the molecular transition energy Ω_0 for geometry A (molecular layer covers the upper wire only). Panels (c) and (d) show energies of all resonances for geometry B (molecular layer covers two lower parallel wires). The asymmetry parameter S = 0 for panels (a) and (c), and S = 20 nm for panels (b) and (d). Note that each resonance is represented by circles with different colors. Horizontal dashed lines in each panel show corresponding non-interacting plasmon modes. For the symmetric case S = 0 there is only one plasmon state, while at S = 20 nm there are two states, as discussed in Figure 1.

wire is at 1.57364 eV, while in ref 10 it is near 1.6 eV. The discrepancy comes from the fact that in our simulations the length of each wire was set to 60 nm (as opposed to 100 nm in ref 10), leading to a higher energy of dipole oscillations. Although a slight offset of the dipole and dark modes results in lower overall coupling since both resonances are sufficiently broad, the strong coupling regime between these modes is clearly observed. We believe that major factors leading to a discrepancy between our results and ref 10 are mainly due to different dielectric constants and cross-sectional geometries. Wires with a square cross section were used in ref 10, while cylinders are used in our work.

Calculations of spatial distributions of the charge density for corresponding dipole and quadrupole modes (not shown) lead to qualitatively similar results to those reported in ref 10. For a nonzero asymmetry parameter S the dipole mode is highly pronounced in the upper wire with surface charges oscillating on both sides of the wire out of phase. This mode is coupled to the quadrupole mode supported by two lower parallel wires, which results in the dip (antiresonance) in the reflection spectra.

RESULTS AND DISCUSSION

The main goal of this work is to explore how the presence of resonant molecular aggregates influences coupling between bright and dark modes in the system shown in Figure 1. We investigate two scenarios of a deposition of molecular aggregates. First (geometry A) is to cover the upper wire with a thin layer of resonant molecules to alter the dipole mode, which in turn changes the indirect coupling between the incident field and the dark mode of the system. The second scenario (geometry B) is to place molecules on a surface of two parallel lower wires in order to see if a resonant molecular system can more efficiently change the coupling by interacting with the dark mode directly. Moreover the spatial proximity of resonant molecular layers in the case of geometry B should lead to a degenerate molecular state and hence more than three modes in the spectra at the strong coupling conditions.

Linear Optical Response. First we examine spectral features of the hybrid system (plasmons+excitons) in the linear regime, calculating reflection as a function of the incident photon energy. The linear regime in our calculations corresponds to molecular excited state populations always much smaller than 1.

Results for both molecular coverages are shown in Figure 2 for the case of a molecular resonance centered at Ω_0 = 1.6 eV. We note several interesting observations. The arrangement corresponding to geometry A shows a clear signature of the strong coupling between molecules and the dipole mode due to strong local field enhancement as it was initially anticipated. For the symmetric orientation of the upper wire, S = 0, one can see that the Rabi splitting of the dipole resonance is about 97 meV. For asymmetric cases the splitting increases, reaching the value of 158 meV at S = 20 nm. It is also clear from Figure 2a that asymmetric arrangements of wires have three distinct resonant

DOI: 10.1021/acsphotonics.5b00146
ACS Photonics 2015, 2, 935−941

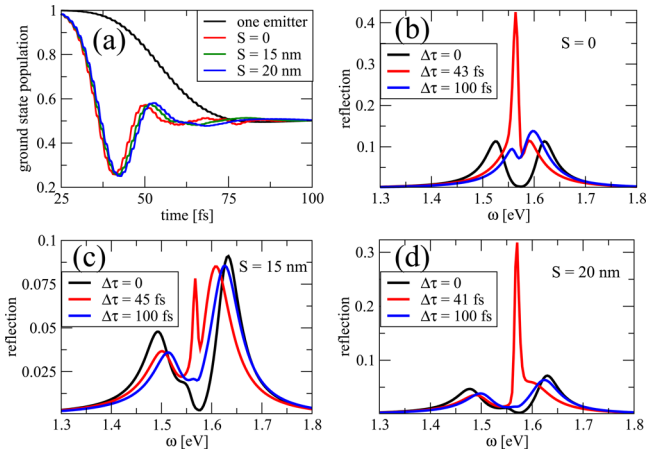

Figure 4. Pump−probe simulations for geometry A. (a) Time dynamics of the ground-state population. Black lines show data for a single molecule under vacuum subject to the pump pulse. Red, green, and blue lines show ensemble average populations of the ground state as a function of time for S = 0 nm, S = 15 nm, and S = 20 nm, respectively. (b) Reflection as a function of the probe photon energy with S = 0 at three pump−probe time delays: black line is for $\Delta\tau$ = 0 (system is not altered by pump yet), red line is for $\Delta\tau$ = 43 fs (panel (b)), $\Delta\tau$ = 45 fs (panel (c)), $\Delta\tau$ = 41 fs (panel (d)), and blue line is for $\Delta\tau$ = 100 fs. Panels (c) and (d) show data similar to that presented in panel (b) but for S = 15 nm and S = 20 nm, respectively. The pump pulse parameters are a pulse duration of 100 fs, a peak amplitude of E_0 = 2.7483 × 10^8 V/m, and a central frequency of 1.57 eV. The molecular transition energy is 1.57 eV.

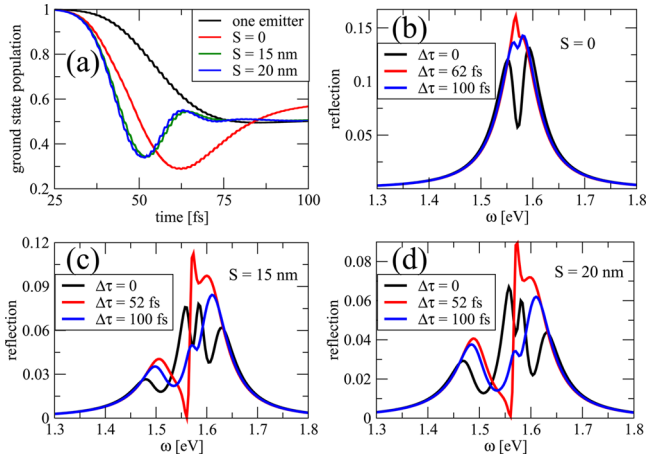

Figure 5. Same as in Figure 4 but for geometry B. Parameters of the molecular system and the pump are the same.

modes corresponding to two obvious hybrid exciton−plasmon modes due to the coupling between molecules and the dipole mode of the upper wire and the dark mode as expected.

In comparing our results (Figure 2) with the electromagnetic transparency window and energy storage results for the asymmetric structure in ref 10, we note a reduction in intensity for both the A and B coating suppositions in our system for S = 0, as expected, although larger than the reduction in intensity of more than 50% that was calculated for the strong coupling regime for the system in ref 10. This has been rationalized in terms of the radiative and nonradiative decay contributions. It is interesting to note that in the case of S = 0, where the strong coupling with the molecular layer induces a Rabi splitting, subsystem B demonstrates a blue-shift for the first peak as compared to subsystem A and the splitting is less pronounced, as is expected. This introduces another parameter that could enable modulation of the reflectance in these geometries.

One may anticipate that for geometry B with two lower wires covered with resonant molecules would exhibit additional interaction: molecular layer on wire 1 with molecular layer on wire 2. If the coupling between these layers and either the dipole mode or the dark mode is strong, the spectral response may show four resonances. The results for geometry B are shown in Figure 2b. For the symmetric case, S = 0, we again observe the Rabi splitting, but this time it is noticeably smaller, 50 meV, compared to the previous case. This can be explained by the fact that the molecular layers now cover two lower wires and its EM coupling to the dipole mode supported by the upper wire is lower. For asymmetric arrangements there are four clearly distinctive resonances observed. This indicates the strong coupling between all four subsystems: the dipole mode of the upper wire, the quadrupole mode of the two parallel lower wires, the molecular aggregate on wire 1, and the molecular aggregate on wire 2. The two last modes are degenerate, with the degeneracy lifted by their coupling with plasmon states of the three interacting wires.

To further demonstrate the physics of such a system, we performed a series of simulations varying the molecular resonant energy Ω_0 for both geometries A and B and extracting energies of each mode for a given molecular transition energy. The results are presented in Figure 3. Both geometries A and B with the symmetric arrangement S = 0 (Figure 3a and c) exhibit a single avoided crossing, indicating the coupling between molecular aggregates and the dipole mode supported by the upper wire. Once the symmetry is broken (S = 20 nm, Figure 3b and d), a set of multiple avoided crossings appears. In the case of geometry A, a single molecular state is coupled to both dipole-dark plasmon states as Figure 3b demonstrates with clearly distinct avoided crossings. Geometry B, with a nonzero asymmetry parameter S, exhibits more complex spectra (Figure 3d). At low and high molecular transition energies both molecular layers show a single resonance due to a weak interaction between them. However, when the molecular energy of both layers approaches the region of the strong coupling with hybrid plasmon states, the degeneracy is removed and spectra show four distinct resonances. It is interesting to note that when the molecular energy is about 1.57 eV (close to the dark plasmon mode), one of the molecular states is very narrow. The proximity of a narrow and a wide resonance could be used to coherently control the EM energy distribution in such a system if properly altered by a strong external laser pulse inducing Fano-type interference.

Pump−Probe Simulations. We consider a pump−probe experiment during which a system under consideration is subject to strong external laser radiation resonant with the molecular aggregate transition. After some time delay, $\Delta\tau$, a low intense probe pulse, arrives and "measures" the corresponding *linear* response of the system altered by the pump. Numerical aspects of such simulations for hybrid plasmon−exciton systems can be found in ref 12. In all simulations presented below we define the pump−probe time delay such that $\Delta\tau$ = 0 corresponds to the probe arriving just before the pump. We note that in actual transient absorption experiments the time resolution is quite limited but still allows one to observe quantum dynamics even within a pump pulse, as was recently reported in ref 7. In this sense our "probe" presents a modeling way of determining an instantaneous quantum state of a system

DOI: 10.1021/acsphotonics.5b00146
ACS Photonics 2015, 2, 935−941

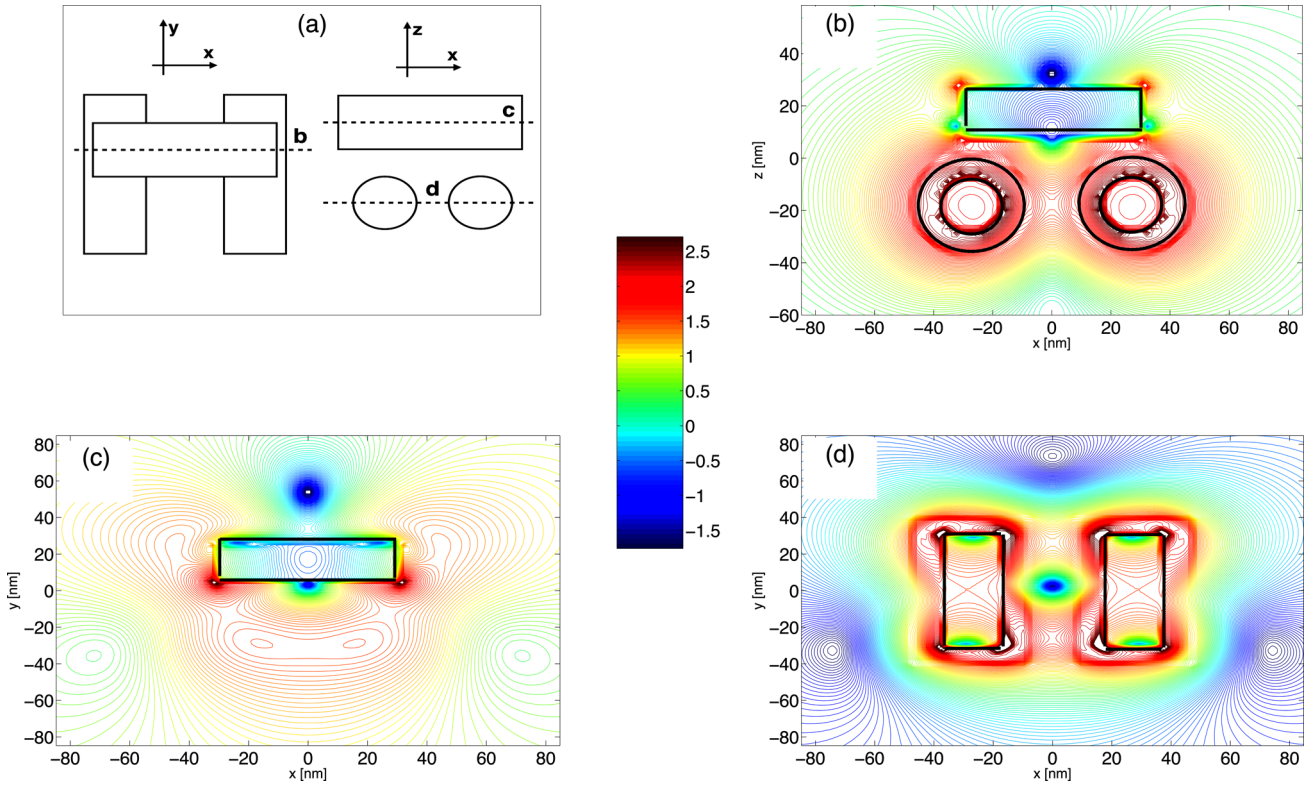

Figure 6. Steady-state electromagnetic intensity distribution calculated for ω = 1.560 49 eV corresponding to the minimum in the reflection spectrum shown in Figure 5c, red line (S = 15 nm, geometry B). (a) Schematics of two-dimensional cuts with each dashed line indicating the corresponding plane, at which intensity is plotted in other panels. (b−d) Intensity distributions plotted in logarithmic scale normalized with respect to the incident intensity, i.e., units of intensity enhancement. Black contour lines depict actual wires along with molecular layers. The incident field is polarized along x and propagates in the negative z direction.

inside the pump. In all simulations presented below the pump pulse is taken resonant with the molecular aggregate transition.

First we examine geometry A, pumping it with a 100 fs laser pulse with an amplitude corresponding to a $\pi/2$-pulse (i.e., pumping half of a molecular population into the excited state). The results of the simulations are presented in Figure 4. Panel (a) shows the time dynamics of the average populations of the molecular ground state compared to a single-molecule case under vacuum. One can see that the dynamics of the hybrid system is significantly different from a single-emitter case: it is noticeably faster, exhibiting several Rabi cycles with diminishing amplitude. We note that observed faster dynamics can be explained by local field enhancement due to the excitation of a corresponding plasmon mode. Higher local field increases the pump pulse area, leading to more Rabi cycles. Another important aspect to point out is a quick decay of the amplitude of the Rabi oscillations. Upon careful examination of spatial distributions of excited molecules, one can conclude that the excitation travels fast, spreading over the entire molecular layer. Since the layer is not uniformly exposed to the pump, this excitation is highly inhomogeneous, leading to a quick dephasing of macroscopic polarization currents.[6] Another evidence to support this explanation is that the Rabi splitting at the end of the pump is considerably lower compared to its unperturbed value (for S = 0 the splitting is 94 meV for the unperturbed spectrum and is only 42 meV at the end of the pump). The excitation spreads quickly over the entire molecular layer, thus leading to a high dephasing, which in turn lowers the coupling with the hybrid plasmon mode and hence affects the Rabi splitting.

To scrutinize the pump dynamics further, we probe the perturbed system at different times, as shown in Figure 4b, c, and d. The system undergoes a strong transition near 40−50 fs, as seen in Figure 4a as a deep minimum of the ground-state population, which reaches almost 20%. Probing the system at these times reveals that the molecular aggregate transitions into the excited state. The reflection spectra calculated around $\Delta\tau$ = 40 fs exhibit a narrow resonance at the molecular transition energy 1.57 eV as the system releases the energy it stored due to the pump. Probed at later times the system shows less and less transitions occurring at 1.57 eV as the excitation quickly dephases, as seen from blue lines in Figure 4b, c, and d.

Completely different physics is seen when examining geometry B as shown in Figure 5. First the quantum dynamics of the molecular subsystem (Figure 5a) is noticeably slower compared to its counterpart (Figure 4a). The latter shows that all arrangements with different asymmetry parameters result in similar time dynamics. On the contrary, the symmetric case with S = 0 for geometry B is considerably slower than others. Probing the system with S = 0 at different time delays $\Delta\tau$ shows basically the same trend we noted above; that is, at the time when the average ground-state population has a minimum, the reflection spectrum has a sharp resonance, indicating the fact that a portion of molecules is in the excited state. It again decays very quickly and relaxes back to the unperturbed spectrum due to quick dephasing. However, for all asymmetric cases with S = 15 nm (Figure 5c) and S = 20 nm (Figure 5d) we observe the strong induced Fano-type resonance with the reflection becoming negligibly small at 1.56 eV. As we anticipated in the Linear Optical Response section while

DOI: 10.1021/acsphotonics.5b00146
ACS Photonics 2015, 2, 935−941

discussing avoided crossings, the proximity of sharp and broad overlapping resonances may lead to strong interference, resulting in Fano line shapes. Here the interference is caused by the excitation of one of the hybrid molecular−plasmon states and its strong coupling with another hybrid state. We note that such a highly pronounced Fano line shape with a deep minimum in the reflection leads to high local field enhancement if being excited at the frequency corresponding to this minimum.[26]

To illustrate how the system behaves at frequencies corresponding to very small reflection, as seen in Figure 5c and d, we calculate steady-state electromagnetic energy distributions as shown in Figure 6. First the structure is pumped by a femtosecond pulse and then probed with a time delay of $\Delta\tau$ = 52 fs at a frequency of ω = 1.560 49 eV, corresponding to the minimum in reflection (see Figure 5c, red line). It should be noted that simulations of transmission yield spectra similar to reflection with the same positions of minima and maxima. This suggests that the structure does not scatter the incident radiation and acts as a very efficient absorber. Intensity distributions support this hypothesis, demonstrating high localization of electromagnetic energy in regions occupied by molecules with local intensity enhancement reaching 3 orders of magnitude. As it was proposed in ref 12, one can pump a plexitonic structure with a femtosecond pulse and abruptly turn the pump off at a desired time, leaving the structure in a given state (as in our case turning the pump off after 52 fs, for instance). A properly prepared system would act as an efficient nanoabsorber for a time corresponding to the characteristic relaxation time needed for molecules to decay back to their ground state.

CONCLUSION

We scrutinized optical properties of a hybrid plasmon−exciton system comprising a resonant molecular subsystem and three Au wires supporting a dipole mode that can be coupled to a dark mode in a controllable fashion by variation of a symmetry parameter. It was shown that if two wires are covered with molecular layers, the system exhibits four resonant modes due to asymmetry and lifted degeneracy of the molecular state, while upon having molecular aggregates covering the top wire, three resonant modes appear. Furthermore, we used pump−probe simulations to study the quantum dynamics and possible ways to control plasmon−exciton materials. It was demonstrated that one can design hybrid nanomaterials with highly pronounced Fano resonances using femtosecond lasers that behave as very efficient nanoabsorbers in the visible. The femtosecond optical engineering of plexitonic systems can be used to create materials with desired properties and functionality.

AUTHOR INFORMATION

Corresponding Authors

*E-mail: maxim.sukharev@asu.edu.
*E-mail: ruth.pachter@us.af.mil.

Notes

The authors declare no competing financial interest.

ACKNOWLEDGMENTS

The authors acknowledge support from the Air Force Office of Scientific Research (Summer Faculty Fellowship 2013).

REFERENCES

(1) Manjavacas, A.; Abajo, F. J. G. d.; Nordlander, P. Quantum Plexcitonics: Strongly Interacting Plasmons and Excitons. *Nano Lett.* **2011**, *11*, 2318−2323.
(2) Patra, B. K.; Guria, A. K.; Dutta, A.; Shit, A.; Pradhan, N. Au-SnS Hetero Nanostructures: Size of Au Matters. *Chem. Mater.* **2014**, *26*, 7194−7200.
(3) In, S.; Mason, D. R.; Lee, H.; Jung, M.; Lee, C.; Park, N. Enhanced Light Trapping and Power Conversion Efficiency in Ultrathin Plasmonic Organic Solar Cells: A Coupled Optical-Electrical Multiphysics Study on the Effect of Nanoparticle Geometry. *ACS Photonics* **2015**, *2*, 78−85.
(4) Yadav, A. Localized Surface Plasmon Enhanced Organic Light-Emitting Diodes. *Plasmonics* **2014**, *9*, 1071−1075.
(5) DeLacy, B. G.; Miller, O. D.; Hsu, C. W.; Zander, Z.; Lacey, S.; Yagloski, R.; Fountain, A. W.; Valdes, E.; Anquillare, E.; Soljačić, M.; Johnson, S. G.; Joannopoulos, J. D. Coherent Plasmon-Exciton Coupling in Silver Platelet-J-Aggregate Nanocomposites. *Nano Lett.* **2015**, *15*, 2588−2593.
(6) Vasa, P.; Wang, W.; Pomraenke, R.; Lammers, M.; Maiuri, M.; Manzoni, C.; Cerullo, G.; Lienau, C. Real-Time Observation of Ultrafast Rabi Oscillations between Excitons and Plasmons in Metal Nanostructures with J-Aggregates. *Nat. Photonics* **2013**, *7*, 128−132.
(7) Vasa, P.; Wang, W.; Pomraenke, R.; Maiuri, M.; Manzoni, C.; Cerullo, G.; Lienau, C. Optical Stark Effects in *J*-Aggregate−Metal Hybrid Nanostructures Exhibiting a Strong Exciton-Surface-Plasmon-Polariton Interaction. *Phys. Rev. Lett.* **2015**, *114*, 036802.
(8) Schlather, A. E.; Large, N.; Urban, A. S.; Nordlander, P.; Halas, N. J. Near-Field Mediated Plexcitonic Coupling and Giant Rabi Splitting in Individual Metallic Dimers. *Nano Lett.* **2013**, *13*, 3281−3286.
(9) Faucheaux, J. A.; Stanton, A. L. D.; Jain, P. K. Plasmon Resonances of Semiconductor Nanocrystals: Physical Principles and New Opportunities. *J. Phys. Chem. Lett.* **2014**, *5*, 976−985.
(10) Gallinet, B.; Siegfried, T.; Sigg, H.; Nordlander, P.; Martin, O. J. F. Plasmonic Radiance: Probing Structure at the Ångström Scale with Visible Light. *Nano Lett.* **2013**, *13*, 497−503.
(11) Salomon, A.; Gordon, R. J.; Prior, Y.; Seideman, T.; Sukharev, M. Strong Coupling between Molecular Excited States and Surface Plasmon Modes of a Slit Array in a Thin Metal Film. *Phys. Rev. Lett.* **2012**, *109*, 073002.
(12) Sukharev, M.; Seideman, T.; Gordon, R. J.; Salomon, A.; Prior, Y. Ultrafast Energy Transfer between Molecular Assemblies and Surface Plasmons in the Strong Coupling Regime. *ACS Nano* **2014**, *8*, 807−817.
(13) Sukharev, M. Control of Optical Properties of Hybrid Materials with Chirped Femtosecond Laser Pulses under Strong Coupling Conditions. *J. Chem. Phys.* **2014**, *141*, 084712.
(14) Antosiewicz, T. J.; Apell, S. P.; Shegai, T. Plasmon-Exciton Interactions in a Core-Shell Geometry: From Enhanced Absorption to Strong Coupling. *ACS Photonics* **2014**, *1*, 454−463.
(15) Miroshnichenko, A. E.; Flach, S.; Kivshar, Y. S. Fano Resonances in Nanoscale Structures. *Rev. Mod. Phys.* **2010**, *82*, 2257−2298.
(16) Verellen, N.; Sonnefraud, Y.; Sobhani, H.; Hao, F.; Moshchalkov, V. V.; Dorpe, P. V.; Nordlander, P.; Maier, S. A. Fano Resonances in Individual Coherent Plasmonic Nanocavities. *Nano Lett.* **2009**, *9*, 1663−1667.
(17) Giannini, V.; Francescato, Y.; Amrania, H.; Phillips, C. C.; Maier, S. A. Fano Resonances in Nanoscale Plasmonic Systems: A Parameter-Free Modeling Approach. *Nano Lett.* **2011**, *11*, 2835−2840.
(18) Bonakdar, A.; Mohseni, H. Impact of Optical Antennas on Active Optoelectronic Devices. *Nanoscale* **2014**, *6*, 10961−10974.
(19) Gray, S. K.; Kupka, T. Propagation of Light in Metallic Nanowire Arrays: Finite-Difference Time-Domain Studies of Silver Cylinders. *Phys. Rev. B* **2003**, *68*, 045415.
(20) Rakić, A. D.; Djurišić, A. B.; Elazar, J. M.; Majewski, M. L. Optical Properties of Metallic Films for Vertical-Cavity Optoelectronic Devices. *Appl. Opt.* **1998**, *37*, 5271−5283.

DOI: 10.1021/acsphotonics.5b00146
ACS Photonics 2015, 2, 935−941

(21) Siegman, A. E. *Lasers*; University Science Books: Mill Valley, CA, 1986.
(22) Puthumpally-Joseph, R.; Atabek, O.; Sukharev, M.; Charron, E. Theoretical Analysis of Dipole-Induced Electromagnetic Transparency. *Phys. Rev. A* **2015**, *91*, 043835.
(23) Taflove, A.; Hagness, S. *Computational Electrodynamics: The Finite-Difference Time-Domain Method*; Artech House, 2000.
(24) Roden, J. A.; Gedney, S. D. Convolution PML (CPML): An Efficient FDTD Implementation of the CFS-PML for Arbitrary Media. *Microwave Opt. Technol. Lett.* **2000**, *27*, 334−339.
(25) Sukharev, M.; Nitzan, A. Numerical Studies of the Interaction of an Atomic Sample with the Electromagnetic Field in Two Dimensions. *Phys. Rev. A* **2011**, *84*, 043802.
(26) Stockman, M. I. Nanoplasmonics: Past, Present, and Glimpse into Future. *Opt. Express* **2011**, *19*, 22029−22106.

DOI: 10.1021/acsphotonics.5b00146
ACS Photonics 2015, 2, 935−941